Title
TGFβ attenuates tumour response to PD-L1 blockade by contributing to exclusion of T cells.

Journal
Nature, 554(7693)

ISSN
0028-0836

Authors
Mariathasan, Sanjeev
Turley, Shannon J
Nickles, Dorothee
et al.

Publication Date
2018-02-01

DOI
10.1038/nature25501

Peer reviewed

HHS Public Access

Author manuscript

Nature. Author manuscript; available in PMC 2018 August 14.

Published in final edited form as:

Nature. 2018 February 22; 554(7693): 544–548. doi:10.1038/nature25501.

TGF-β attenuates tumour response to PD-L1 blockade by contributing to exclusion of T cells

Sanjeev Mariathasan[1,*,^], **Shannon J. Turley**[1,*,^], **Dorothee Nickles**[1,*], **Alessandra Castiglioni**[1], **Kobe Yuen**[1], **Yulei Wang**[1], **Edward E. Kadel III**[1], **Hartmut Koeppen**[1], **Jillian L. Astarita**[1], **Rafael Cubas**[1], **Suchit Jhunjhunwala**[1], **Romain Banchereau**[1], **Yagai Yang**[1], **Yinghui Guan**[1], **Cecile Chalouni**[1], **James Ziai**[1], **Yasin Şenbabaoğlu**[1], **Stephen Santoro**[1], **Daniel Sheinson**[1], **Jeffrey Hung**[1], **Jennifer M. Giltnane**[1], **Andrew K. Pierce**[1], **Kathryn Mesh**[1], **Steve Lianoglou**[1], **Johannes Riegler**[1], **Richard A. D. Carano**[1], **Pontus Eriksson**[2], **Mattias Hoglund**[2], **Loan Somarriba**[3], **Daniel L. Halligan**[3], **Michiel van der Heijden**[4], **Yohann Loriot**[5], **Jonathan E. Rosenberg**[6], **Lawrence Fong**[7], **Ira Mellman**[1], **Daniel S. Chen**[1], **Marjorie Green**[1], **Christina Derleth**[1], **Gregg D. Fine**[1], **Priti S. Hegde**[1], **Richard Bourgon**[1,^], and **Thomas Powles**[8]

[1]Genentech, South San Francisco, California 94080, USA [2]Division of Oncology and Pathology, Department of Clinical Sciences Lund, Lund University, Lund, Skåne, SE-223 81, Sweden [3]Fios Genomics, Edinburgh, Scotland EH16 4UX, UK [4]Netherlands Cancer Institute, 1066 CX Amsterdam, The Netherlands [5]Department of Cancer Medicine, Institut Gustave Roussy, University of Paris Sud, 94800 Villejuif, France [6]Genitourinary Oncology Service, Department of Medicine, Memorial Sloan Kettering Cancer Center, New York, New York 10065, USA [7]University of California San Francisco, Helen Diller Family Comprehensive Cancer Center, San Francisco, California 94158, USA [8]Barts Experimental Cancer Medicine Centre, Barts Cancer Institute, Queen Mary University of London, London EC1M 6BQ, UK

Abstract

^Co-corresponding authors: Sanjeev Mariathasan, mariathasan.sanjeev@gene.com; Shannon Turley, turley.shannon@gene.com; Richard Bourgon, bourgon.richard@gene.com.

*These authors contributed equally to this work.

Author contributions

SM, SJT, DN, JR, LF, IM, DSC, MG, CD, GDF, PSH, RB, TP contributed to the overall study design. SM, SJT, DN, YW, EEK, KY, YG, YS, SL, PE, MH, LS, DLH, PSH, RB performed the biomarker and statistical analyses. HK, CC, JZ, SS, DS, JH, JMG, AKP, KM conducted microscopy studies. SJT, AC, JA, RC designed all the preclinical experiments, SJT, AC, JA, RC, YY, CC, JZ, YS, SS, DS, JH, JMG, AKP, KM, JR, RADC analysed the corresponding preclinical data. SM, SJT, DN, IM, PSH, RB, TP wrote the paper. All authors contributed to data interpretation, discussion of results and commented on the manuscript.

Additional information

All raw sequencing data required for RNAseq analyses have been deposited to the European Genome-Phenome Archive under accession number EGAS#00001002556. In addition, the source code and processed data used for all analyses presented here have been made available in *IMvigor210CoreBiologies*, a fully documented software and data package for the R statistical computing environment (R Core Team, 2016. R: A language and environment for statistical computing. R Foundation for Statistical Computing, Vienna, Austria. https://www.r-project.org). This package is freely available under the Creative Commons 3.0 license and can be downloaded from http://research-pub.gene.com/IMvigor210CoreBiologies.

Conflicts of interest

Pontus Eriksson, Mattias Hoglund, Lawrence Fong, Stephen Santoro have no competing interests.

Therapeutic antibodies that block the programmed death-ligand 1 (PD-L1)/programmed death-1 (PD-1) pathway can induce robust and durable responses in patients with various cancers, including metastatic urothelial cancer (mUC)[1–5]. However, these responses only occur in a subset of patients. Elucidating the determinants of response and resistance is key to improving outcomes and developing new treatment strategies. Here, we examined tumours from a large cohort of mUC patients treated with an anti–PD-L1 agent (atezolizumab) and identified major determinants of clinical outcome. Response was associated with CD8+ T-effector cell phenotype and, to an even greater extent, high neoantigen or tumour mutation burden (TMB). Lack of response was associated with a signature of transforming growth factor β (TGF-β) signalling in fibroblasts, particularly in patients with CD8+ T cells that were excluded from the tumour parenchyma and instead found in the fibroblast- and collagen-rich peritumoural stroma—a common phenotype among patients with mUC. Using a mouse model that recapitulates this immune excluded phenotype, we found that therapeutic administration of a TGF-β blocking antibody together with anti–PD-L1 reduced TGF-β signalling in stromal cells, facilitated T cell penetration into the centre of the tumour, and provoked vigorous anti-tumour immunity and tumour regression. Integration of these three independent biological features provides the best basis for understanding outcome in this setting and suggests that TGF-β shapes the tumour microenvironment to restrain anti-tumour immunity by restricting T cell infiltration.

Pre-treatment tumour samples from a large phase 2 trial (IMvigor210) investigating the clinical activity of PD-L1 blockade with atezolizumab in mUC were used for an integrated biomarker evaluation (Extended Data Fig. 1a; Supplemental Discussion). Here, patients who achieved a complete response (CR) or partial response (PR) were categorised as responders and compared with non-responders, who displayed stable (SD) or progressive disease (PD). As found previously[2,4], PD-L1 expression on IC (>5% of cells with SP142 antibody) was significantly associated with response (Fig. 1a). In contrast, PD-L1 expression on tumour cells (TC) was not associated with response (Extended Data Fig. 1b). We next performed transcriptome RNA sequencing in 298 tissue samples and assessed correlation with PD-L1 expression on IC and with response. A gene set associated with CD8+ T-effector (T_{eff}) cells[4,5] was highly correlated with IC (Extended Data Fig. 1c,d; Supplemental Discussion). It was also significantly associated with response, particularly with CR, and with overall survival (Fig. 1b,c).

mUC is characterised by one of the highest somatic mutation rates[6,7]. In mUC, TMB correlates with response to immune checkpoint inhibitors[4,5]. We confirmed these findings (Fig. 1d,e) and showed that computationally predicted tumour neoantigen burden behaved similarly (Extended Data Fig. 1e,f), suggesting that the relevance of TMB reflects an increased potential for immunogenicity[8–11]. We next assessed the transcriptional and mutational correlates of TMB in mUC. The pathways most significantly associated with TMB were those involved in cell cycle, DNA replication and DNA damage response (DDR, Extended Data Fig. 1g, Supplementary Table S1). Signatures for these pathways were correlated with *MKI67* and thus with proliferation (Extended Data Fig. 1h). Expression levels for *APOBEC3A* and *APOBEC3B*, two cytidine deaminases up-regulated in urothelial and other cancers[12,13], were also correlated with TMB and response (Extended Data Fig. 1i,j; Supplementary Tables S2 and S3). Finally, tumours with one or more mutations in DDR

or cell cycle regulator gene sets gene set had significantly higher TMB and response rates (Fig. 1f,g; Extended Data Fig. 1k,l; Supplementary Tables S4,S5).

Next, we sought features beyond CD8+ T-cell immunity and TMB that associated with response. Gene set enrichment analysis identified the cytokine-cytokine receptor gene set as the sole feature associated with non-response (Extended Data Fig. 2a, Supplementary Table S6). The most significantly associated genes within this pathway were *IFNGR1* and genes involved in the TGF-β signalling pathway: *TGFB1*, *ACVR1* and *TGFBR2* (Supplementary Table S3). While IFN-γ is known to have favourable effects on anti-tumour immunity, persistent signalling by to this cytokine has been associated with adaptive resistance to checkpoint therapy[14–17]. We observed significantly enhanced expression of IFN-γ in responders, whereas *IFNGR1* expression was significantly higher in non-responders (Extended Data Fig. 2b,c). TGF-β is a pleiotropic cytokine associated with poor prognosis in multiple tumour types[18–20], and it is thought to play a pro-tumorigenic role in advanced cancers by promoting immunosuppression, angiogenesis, metastasis, tumour cell epithelial to mesenchymal transition (EMT), fibroblast activation and desmoplasia[19,21–23]. In our data, the two top-scoring TGF-β pathway genes represent a TGF-β ligand, *TGFB1*, and a TGF-β receptor, *TGFBR2*. Both showed increased mean expression in non-responders and association with reduced overall survival (Fig. 1h,i; Extended Data Fig. 2d,e). Taken together, these results suggest that the impact of checkpoint inhibition on patient outcome in mUC is dictated by three core biological pathways: (i) pre-existing T-cell immunity and (ii) TMB are positively associated with outcome, whereas (iii) TGF-β is associated with lack of response and reduced survival (Fig. 1j).

Most human solid tumours exhibit one of three distinct immunological phenotypes: *immune inflamed*, *immune excluded*, or *immune desert*[1,24]. Data, largely from melanoma, have suggested that inflamed tumours are most responsive to checkpoint blockade[24,25], but the relevance of tumour-immune phenotype to mUC response was previously unknown. In our mUC cohort, a significant proportion of tumours (47%) exhibited the excluded phenotype, whereas desert and inflamed tumours comprised only 27% and 26% (Extended Data Fig. 2f; Fig. 2a,b). Average signal for the CD8+ T_{eff} signature was lowest in desert, intermediate in excluded, and highest in inflamed tumours (Fig. 2c), and was significantly associated with response in inflamed tumours only, consistent with a model in which the absence of CD8+ T cells, or their spatial separation from tumour cells, makes the signature irrelevant.

The observed proximity of CD8+ T cells to desmoplastic stroma in immune excluded tumours (Extended Data Fig. 2f; Fig. 2a) suggests that the relevance of TGF-β in this phenotype may be driven by its impact on stromal cells. To measure TGF-β pathway activity specifically in fibroblasts, we generated a pan-fibroblast TGF-β response signature (Pan-F-TBRS). Average expression for this signature was low in immune deserts but significantly higher in inflamed and excluded tumours. Consistent with a role for TGF-β pathway activation in TME fibroblasts, the Pan-F-TBRS was significantly associated with non-response in excluded tumours only (Fig. 2d). TMB was significantly associated with response in both excluded and inflamed tumours (Fig. 2e).

To better understand how the three core pathways relate to one another and to reveal their relative strengths of association with outcome, a statistical analysis of competing models was performed. Logistic regression pseudo-R^2 was used as a measure of "explained variance" in patient response[26].

In immune desert tumours, the pathways showed negligible explanatory power (Fig. 2f). For excluded tumours, both the Pan-F-TBRS signature and TMB were significantly associated with response, and combining the two provided a significant improvement over either term alone. For inflamed tumours, on the other hand, the CD8+ T_{eff} signature combined with TMB gave the strongest correlation with response. In an analysis using all samples together, a model incorporating each core pathway significantly improved on all singleton and two-pathway models (Fig. 2f, Extended Data Fig. 2g), demonstrating that the information provided by each pathway is at least partially independent.

The Cancer Genome Atlas (TCGA) molecular subtype taxonomy[12] has been widely investigated in mUC, but with inconsistent results. Here we contrast the TCGA taxonomy with the Lund taxonomy, which includes a genomically unstable (GU) subtype[27,28] (Extended Data Fig. 3). Consistent with the importance of TMB, we observed that the GU subtype was significantly enriched for response (Fig. 3). This effect could not, however, be attributed to TMB alone, as the TCGA luminal II subtype was similarly enriched for high-TMB tumours (Extended Data Fig. 4a,b). Instead, we identified the source of the difference by separately evaluating patients classified as TCGA luminal II only, Lund GU only, or both (Extended Data Fig. 4c). GU-only tumours had the lowest CD8+ T_{eff} signature scores and lowest TMB but responded favourably; in contrast, luminal II-only tumours showed sharply elevated Pan-F-TBRS scores and responded poorly (Extended Data Fig. 4d,e). These results demonstrate the importance of interplay between the three core pathways in determining response. Further discussion of the Lund subtypes is provided as Supplemental Discussion.

In light of our hypothesis that physical exclusion of T cells by the stromal barrier limits response to atezolizumab in immune excluded tumours, we studied the EMT6 mouse mammary carcinoma model to determine if there was a role for TGF-β–activated stroma in this context. The EMT6 model exhibits the immune excluded phenotype (Extended Data Fig. 5a–d) and also expresses all TGF-β isoforms as well as PD-L1 (Extended Data Fig. 5e,f). Although therapeutic blockade of PD-L1 or TGF-β alone had little or no effect, mice treated with both antibodies exhibited a significant reduction in tumour burden (Fig. 4a,b; Extended Data Fig. 5g,h). Regression of EMT6 tumours in these studies was wholly dependent on CD8+ T cells (Extended Data Fig. 5i). These findings were reproduced in a second relevant mouse tumour model, MC38 (Extended Data Fig. 5j–n).

Dual antibody blockade also led to a significant increase in the abundance of tumour infiltrating T cells (Extended Data Fig. 6a), particularly CD8+ T_{eff} cells (Fig. 4c,d; Extended Data Fig. 6b). Blockade of TGF-β, alone or in combination with anti-PD-L1, had no effect on CD4+ T regulatory (T_{reg}) cells in the tumour (Extended Data Fig. 6c–e). RNA sequencing data revealed that the CD8+ T_{eff} signature was elevated in mouse tumours treated with a combination of anti–PD-L1 plus anti–TGF-β (Fig. 4e). Quantitative histopathology demonstrated that T cell distribution significantly changed following

combination therapy, with mean distance from stromal border increasing, and from tumour centre decreasing. However, T cell localization did not change with either single antibody treatment (Fig. 4f–h, Extended Data Fig. 6f). Together these results suggest that TGF-β inhibition potentiated the ability of anti–PD-L1 to enhance anti-tumour immunity, resulting in optimal T cell positioning and ensuing tumour regression.

Anti-TGF-β treatment significantly reduced TGF-β receptor signalling (i.e. pSMAD2/3) in EMT6 tumours, particularly in non-immune cells (Extended Data Fig. 6g,h). Given that TGF-β is associated with fibroblast differentiation and EMT[22], we asked whether the benefits of dual antibody blockade could be attributed to direct effects on tumour cells or effects on stromal compartments. While single-agent inhibition of TGF-β reduced one of the three EMT signatures we considered, dual antibody treatment had no significant impact (Extended Data Fig. 6i). In contrast, the Pan-F-TBRS score and canonical fibroblast genes associated with matrix remodelling were significantly reduced in the combination treatment (Fig. 4i–l). Consistent with the phospho-flow analysis showing no change in pSMAD2/3 in hematopoietic cells, no reduction was observed in two alternate TBRS signatures associated with T cells or macrophages (Extended Data Fig. 6j,k)[20]. Blockade of TGF-β can thus synergise with anti–PD-L1 in the EMT6 model to reprogram peritumoral stromal fibroblasts and increase CD8+ T_{eff} cell counts in the tumour bed, leading to robust anti-tumour immunity. Interestingly, although TGF-β inhibition might also be expected to diminish T_{reg} cells, diminished T_{reg} numbers were not observed and thus did not appear to contribute to combination efficacy.

The comprehensive evaluation of molecular, cellular and genetic factors associated with response and resistance to checkpoint blockade (atezolizumab) in this large cohort of mUC patients has yielded several important conclusions. Three non-redundant factors were found to contribute: (i) pre-existing immunity, as represented by PD-L1 gene expression on IC, IFNγ-expression, and histological correlates of CD8+ T_{eff} activity; (ii) TMB, measured directly (Extended Data Fig. 7) but also reflected in signatures of proliferation and DNA damage response; and (iii) TGF-β pathway signalling, reflected by a distinct gene expression signature and by pSMAD2/3. These tightly connected findings have not been described previously, and their interrelationship may partially explain why predicting outcome from PD-L1 expression alone is challenging. The enrichment of the fibroblast TGF-β response signature in non-responding immune-excluded tumours, combined with results from Lund molecular subtyping and with preclinical models showing that co-inhibition of TGF-β and PD-L1 converted tumours from an excluded to an inflamed phenotype, support a model in which TGF-β signalling may counteract anti-tumour immunity by restricting the T-cells in the TME. The observed multifactorial basis of response to immunotherapy may be applicable to other tumour types beyond mUC. Work in this area, across multiple tumour types and therapies, is still in its infancy, but these results open new avenues for disease-agnostic exploration of the mechanisms underlying response to and primary immune escape from cancer immunotherapy.

Methods

A full description of all methods is provided as Supplementary Information.

Extended Data

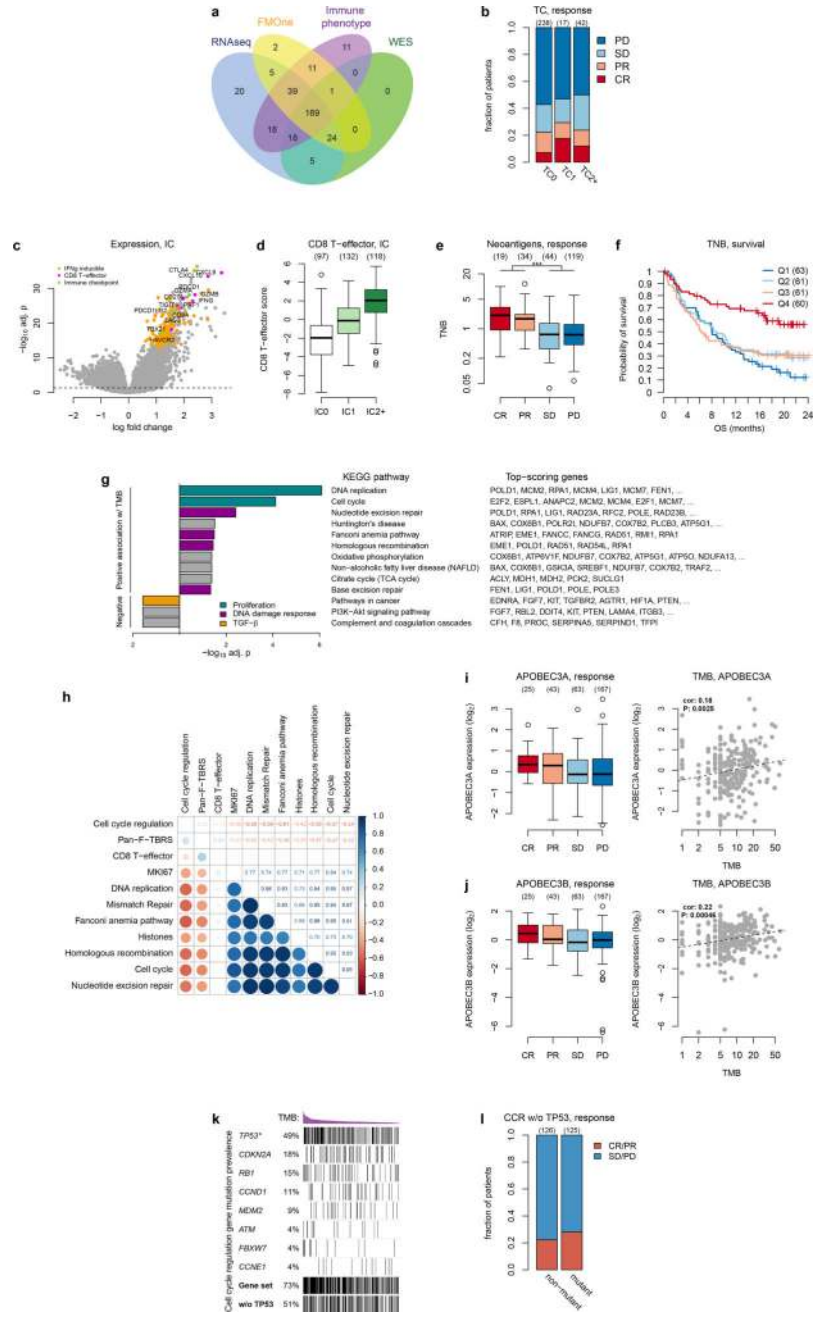

Extended Data Figure 1. Molecular correlates of outcome and tumour mutation burden (TMB)

a, Overlap of the efficacy-evaluable patient populations with assays used in this study (n = 326 for one or more of these assays). For gene expression analyses with respect to response, the complete RNAseq data set was used (n = 298). For gene expression analyses in the context of TMB or immune phenotype, the intersect between RNAseq and FMOne (n = 237) or immune phenotype (n = 244) was used, respectively. For mutation analysis around immune phenotypes, the intersect between FMOne and immune phenotype was used (n = 220). For associations between response or genes mutation status with TMB, the complete

FMOne data set was used ($n = 251$). **b,** PD-L1 protein expression on tumour cells (TC), in contrast to expression on immune cells (IC; Fig. 1a), was not associated with response to atezolizumab (two-sided Fisher exact test; $p = 0.72$). **c–d,** Transcriptional correlates of PD-L1 protein expression on IC. c, Genes associated with PD-L1 immunohistochemistry (IHC) positivity on IC. Normalized $\log_2$-transformed gene expression was compared with PD-L1 IC protein expression. Interferon-stimulated genes[29] and previously reported CD8 T_{eff} and immune checkpoint molecule gene sets[4,5] were among the most up-regulated (complete list of associated genes given in Supplementary Table S10). d, Association between CD8 T_{eff} signature score and PD-L1 IC. There is a significant positive relationship between the signature score and PD-L1 IC staining (likelihood ratio test $p = 4.2 \times 10^{-35}$). **e–f,** Tumour neoantigen burden (TNB) is associated with outcome. e, Box plots showing the relationship between response status and TNB. Shown are number of mutations based on whole-exome sequencing, filtering for those mutations that are predicted to be expressed neoantigens. TNB is positively associated with response to atezolizumab (two-tailed t test $p = 2.7 \times 10^{-9}$). f, TNB, split into quartiles, is also associated with overall survival (OS; likelihood ratio test $p = 0.00015$). **g,** KEGG pathways enriched in genes whose expression is correlated with TMB. Shown are adjusted $-\log_{10} p$ values for enrichment of KEGG gene sets significantly (FDR < 0.05) enriched in genes that are correlated with TMB (272 samples analysed). Sets inferred to reflect key underlying biological processes are coloured. Only the top seven genes per set (ranked by single-gene p value) are shown. **h,** Relationship between different gene expression signatures as well as the single-gene expression values for *MKI67*, a marker for proliferation. In the left corner, correlation between signature scores/gene expression is visualized (348 samples analysed). In the right corner, Pearson correlation coefficients are given. Gene set membership is given in Supplementary Table S8. **i–j,** *APOBEC3A* and *APOBEC3B* gene expression and its association with response and tumour mutation burden (TMB). Both *APOBEC3A* (two-tailed t test $p = 0.015$; i) and *APOBEC3B* (two-tailed t test $p = 0.0025$; j) exhibit higher mean expression in responders. For TMB, Pearson correlation coefficients and p values are given. For j, the two extreme expression outliers were excluded when calculating correlation between gene expression and TMB. **k,** Mutations in cell cycle regulator genes are associated with TMB. Genes are plotted in rows and patients (n = 293) in columns, marking patients with a mutation with a black rectangle. The upper bar plot depicts TMB in each patient. The final rows represent the mutation status of the pathway with or without TP53. Percentages to the left of the plot indicate prevalence. Genes with significant single gene associations with TMB are marked by an asterisk. Mutations in cell cycle regulator genes are associated with TMB with inclusion of *TP53* (two-tailed t test $p = 4.01 \times 10^{-8}$), but not without inclusion of *TP53* (two-tailed t test $p = 0.0652156$; Supplementary Table S4). **l,** Mutation status in cell cycle regulation (CCR) pathway by response. For each patient, it is determined whether they harbour any mutation in a gene belonging to the CCR pathway, except for TP53. Excluding TP53, there is no association between mutation status for the CCR pathway and response (two-sided Fisher test $p = 0.31104$; Supplementary Table S4). Sample sizes given in parentheses. Pan-F-TBRS: pan-fibroblast TGF-β response signature. CR, complete response; PD, progressive disease; PR, partial response; SD, stable disease; TMB, tumour mutation burden.

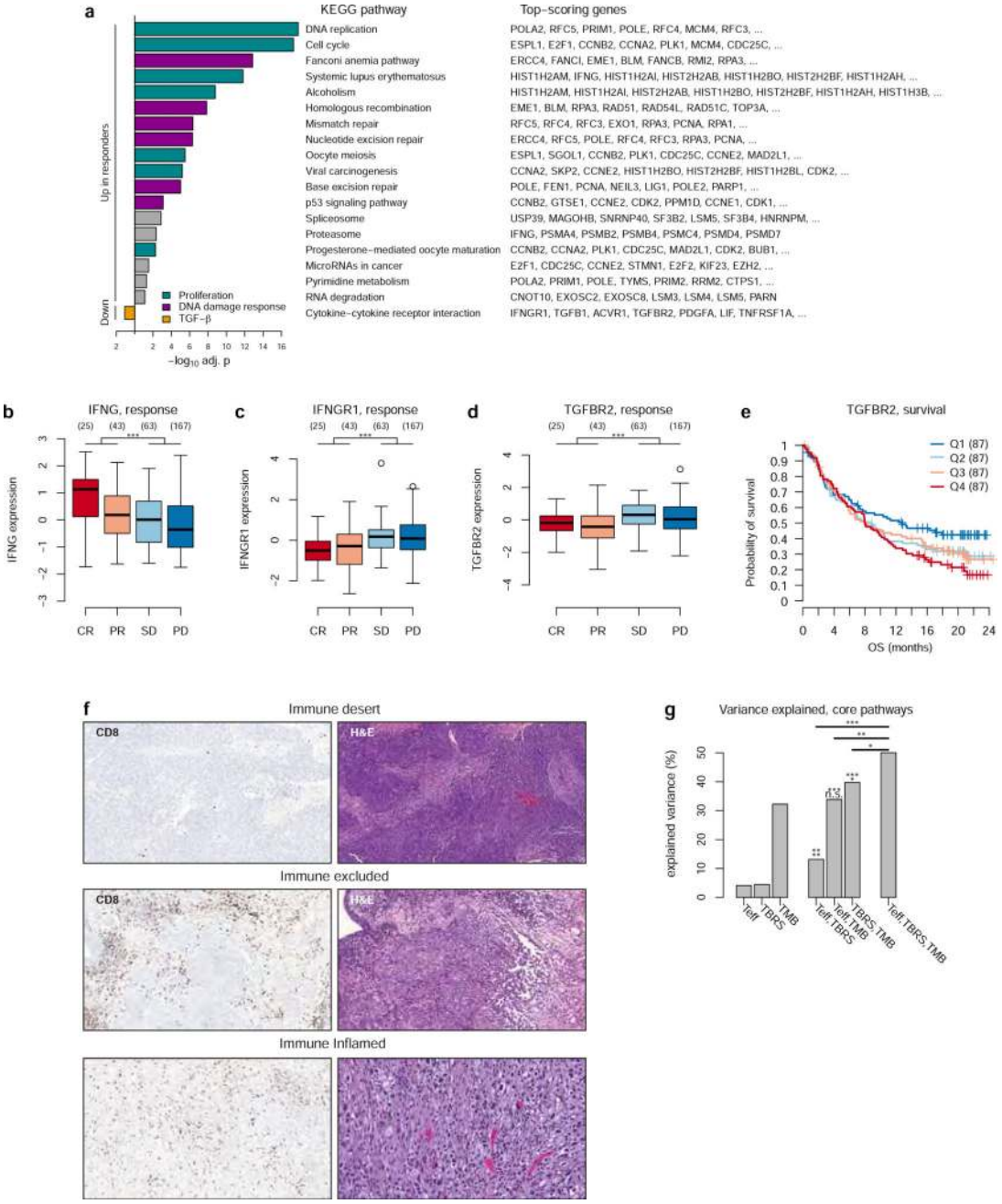

Extended Data Figure 2. Pathways associated with response and cancer-immune phenotypes

a, KEGG pathways significantly associated with response to atezolizumab (adj. $p < 0.10$; comparing 68 responders to 230 non-responders). The top seven genes per set are shown; complete lists are given in Supplementary Table S6. **b–c,** *IFNG* (b) and *IFNGR1* (c) gene expression (y-axis) is significantly associated with response (two-tailed t test $p = 9.1 \times 10^{-5}$) and non-response (two-tailed t test $p = 0.00012$), respectively. **d–e,** *TGFBR2* gene expression (y-axis) is significantly associated with non-response (two-tailed t test $p = 0.00019$, d) and, when split by quartiles, with reduced overall survival (likelihood ratio test p = 0.022, e). b–d: The numbers above the graphs specify sample numbers in each bin. CR,

complete response; PR, partial response; SD, stable disease; PD, progressive disease. e: 87 samples per quartile. Q1: lowest quartile, Q4: highest quartile. **f,** Histology of tumour-immune phenotypes: *desert*, *excluded*, and *inflamed*. **g,** Explained variance in patient response. Generalized linear models were fit to all efficacy-evaluable, immune phenotyped samples (n = 204) using binary response (CR/PR vs SD/PD) as the dependent variable and scores from single input or input combinations (x-axis) as independent variables. Percent explained variance of response is plotted on the y-axis. Comparisons between different models were made via likelihood ratio test. Horizontal bars describe likelihood ratio test results for two-biology vs. three-biology model comparisons. Stacked significance symbols for two-biology models show results of likelihood ratio test comparison to the first single-biology model and separately to the second single-biology model, in the same order as given in bar label on x-axis. (E.g., The T_{eff}, TMB model achieves three stars when compared to the T_{eff} singleton, but an "n.s." when compared to the TMB singleton—due to dilution of its inflamed-specific signal in this all-sample analysis.) A model that includes both DNA (TMB) and RNA markers (CD8+ T_{eff} signature and Pan-F-TBRS) as well as interactions between the Pan-F-TBRS and both TMB and cancer-immune phenotype explains 50% of the variance observed in response, and it significantly improves on all singleton and two-biology models. This final bar is also given on the far right in Fig. 2f. n.s. $p > 0.1$; · $p < 0.1$; * $p < 0.05$; ** $p < 0.01$; *** $p < 0.001$. Exact likelihood ratio test p values: "Teff,TBRS" versus "Teff": 0.0026, "Teff,TBRS" versus "TBRS": 0.0032, "Teff,TMB" versus "Teff": 4.9×10^{-8}, "Teff,TMB" versus "TMB": 0.2, "TBRS,TMB" versus "TBRS": 6.6×10^{-8}, "TBRS,TMB" versus "TMB": 0.014, "Teff,TBRS,TMB" versus "Teff,TBRS": 1.9×10^{-7}, "Teff,TBRS,TMB" versus "Teff,TMB": 0.0028, "Teff,TBRS,TMB" versus "TBRS,TMB": 0.016. Teff: CD8 T effector gene signature, TMB: tumour mutation burden, (Pan-F-)TBRS: pan-tissue fibroblast TGF-β response genes.

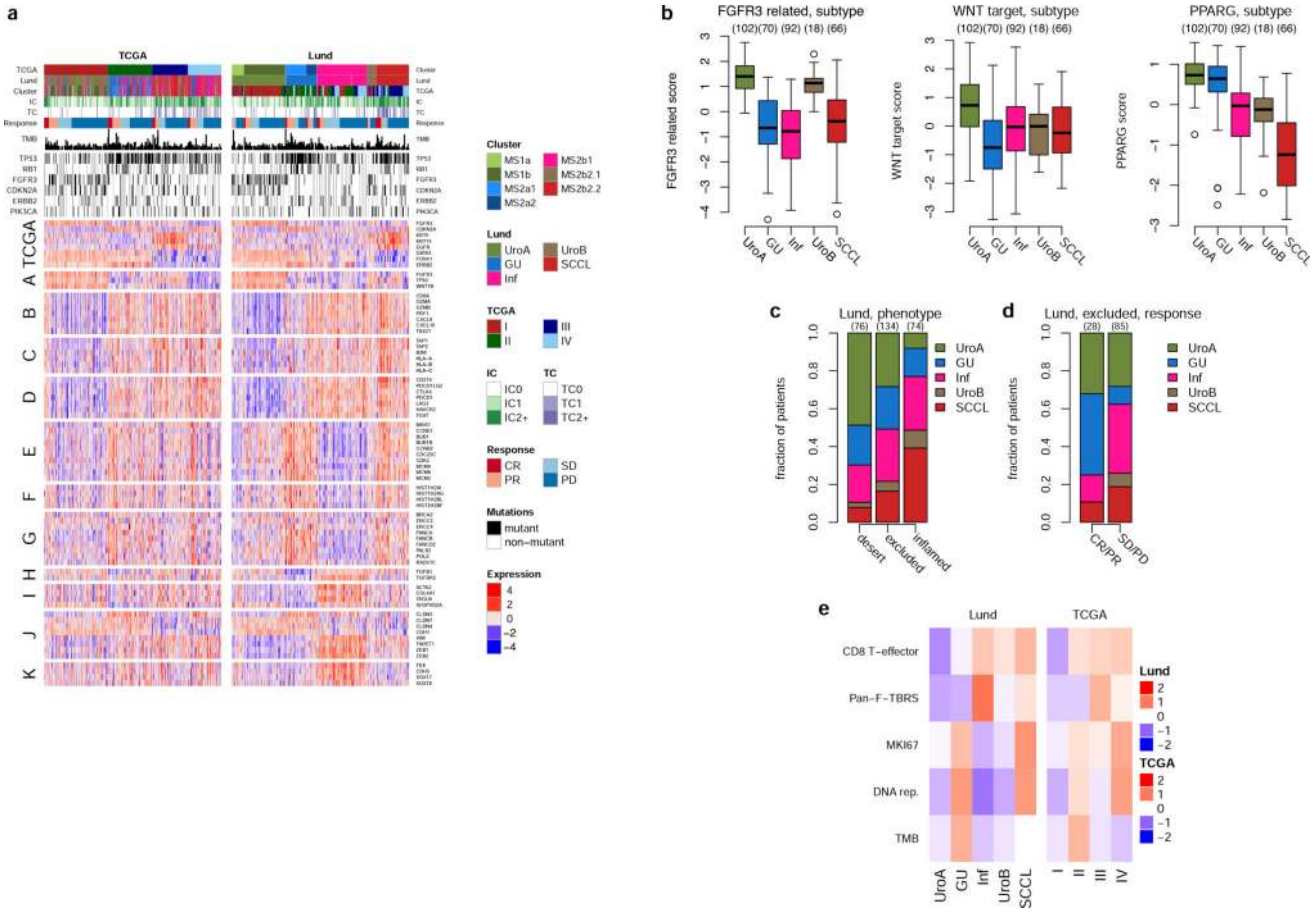

Extended Data Figure 3. Comparison between Lund and TCGA subtyping schemes

a, Heatmap representing all patients evaluated, except for patients without defined response, arranged in columns and sorted first by molecular subtype, then by response to atezolizumab. For the left-hand panel, patients were sorted based on a TCGA-based subtyping scheme, for the right-hand panel, patients were sorted by a Lund-based subtyping scheme (like Fig. 3a). Immune cell (IC) and tumour cell (TC) PD-L1 status are given. In addition, tumour mutation burden (TMB) and mutation status (either mutated, black, or not-mutated; grey: patients without mutation data) for a few genes of interest are shown. The rows of the heatmap show expression (z-scores) of genes of interest, grouped into the following biologies/pathways: TCGA: TCGA subtyping genes, A: *FGFR3* gene signature, B: CD8 T-effector signature, C: antigen processing machinery, D: Immune Checkpoint signature, E: MKI67 and cell cycle genes, F: DNA replication-dependent histones, G: DNA damage repair genes, H: TGF-β receptor and ligand, I: Pan-F-TBRS genes, J: angiogenesis signature, K: epithelial-mesenchymal transition (EMT) markers (for details on these signatures see Methods). CR, complete response; GU, genomically unstable; Inf, infiltrated; PD, progressive disease; PR, partial response; SCCL, basal/SCC-like; SD, stable disease; UroA, urothelial-like A; UroB, urothelial-like B, Pan-F-TBRS: pan-tissue fibroblast TGF-β response genes. **b,** FGFR3-related and WNT target genes[30] as well as *PPARG* are significantly differentially expressed by Lund subtype (Wald p FGFR3-related: 2.7×10^{-43}, WNT target: 1.3×10^{-15}, *PPARG*: 1.2×10^{-53}). Gene set membership is given in

Supplementary Table S8. **c–d,** Distribution of Lund subtypes by cancer-immune phenotypes and response status. c, The fraction of patients within the different Lund subtypes (y-axis) is plotted by tumour-immune phenotype. There is a significant difference in Lund subtype composition between cancer-immune phenotypes (Chi-squared test $p = 1.2 \times 10^{-7}$). d, For excluded tumours, the fraction of patients within the different Lund subtypes (y-axis) is plotted by response status [responders: complete and partial response (CR/PR), non-responders: stable and progressive disease (SD/PD)]. There is a significant difference in Lund subtype composition between response groups (Chi-squared test $p = 0.00061$). The numbers above the graphs specify sample numbers in each bin. **e,** Assessment of *MKI67* expression and signatures of interest as well as TMB relative to molecular subtypes. Biologies of interest were scaled before medians were calculated across the Lund (left) and TCGA (right) molecular subtypes (columns). Red means high, blue means low. CR, complete response; DNA rep., DNA replication; GU, genomically unstable; Inf, infiltrated; PD, progressive disease; PR, partial response; SCCL, basal/SCC-like; SD, stable disease; TMB, tumour mutation burden; UroA, urothelial-like A; UroB, urothelial-like B, Pan-F-TBRS: pan tissue fibroblast TGF-β response signature.

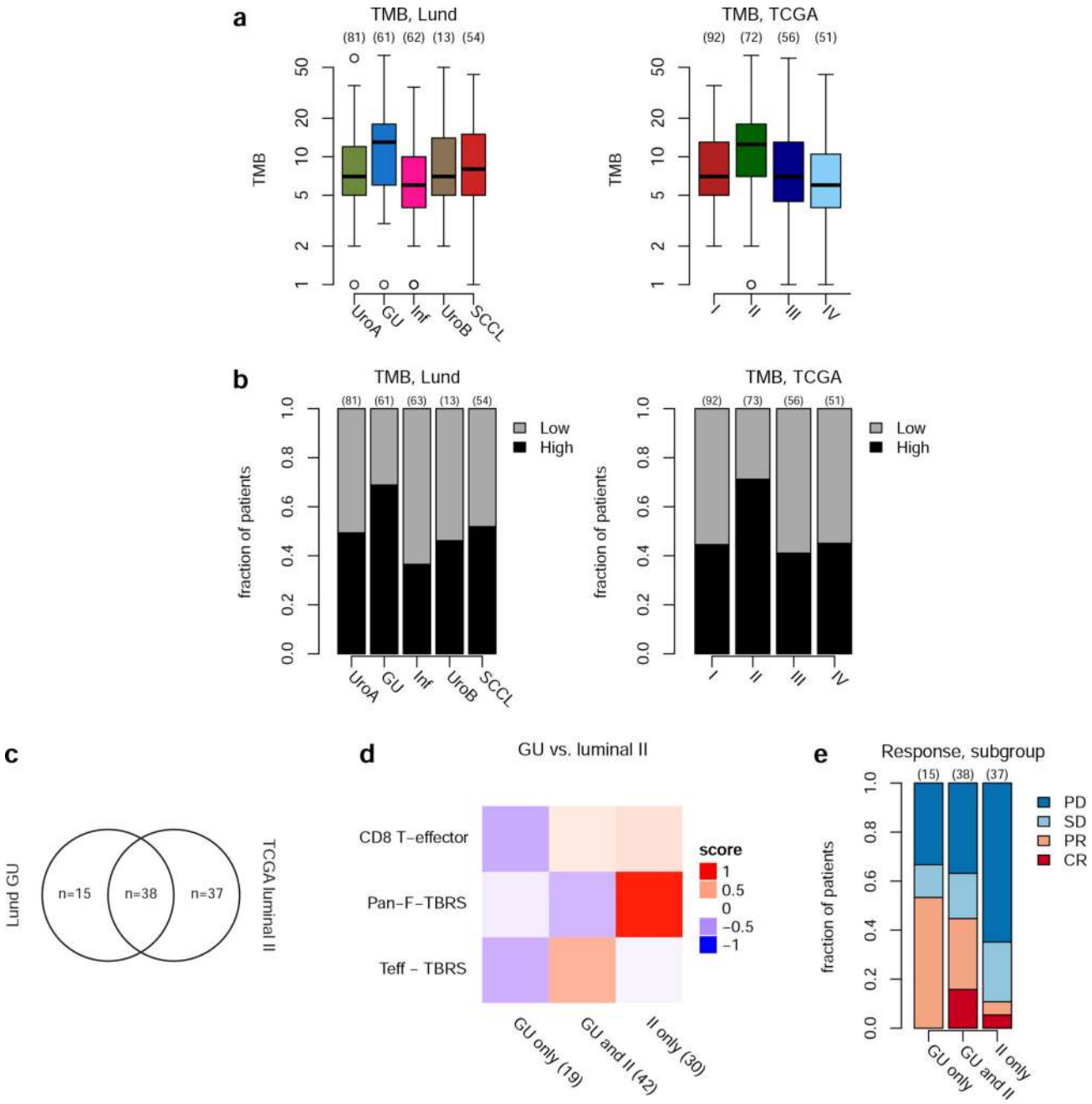

Extended Data Figure 4. Contrasting Lund and TCGA molecular subtyping

a, Tumour mutation burden (TMB; y-axis) is plotted against Lund and TCGA subtypes (x-axis). The Lund genomically unstable (two-tailed t test; $p = 0.00018$) and TCGA luminal II subtypes ($p = 0.00024$) have a higher median TMB. **b,** Patients are split into TMB low (grey) and high (black), based on median TMB, and the fraction of patients in these two groups is shown for the Lund and TCGA molecular subtypes. **c–e,** TGF-β as likely driver of differential response in Lund GU. **c,** Three patient subgroups: Lund GU but not TCGA luminal II, both GU and luminal II, or luminal II but not GU. **d,** CD8+ T_{eff}, Pan-F-TBRS and TMB by subgroup. **e,** Response differs significantly by subgroups (two-tailed Fisher

exact $p = 0.00062$). The numbers above the graphs or in parentheses specify sample numbers in each bin. GU, genomically unstable; Inf, infiltrated; Pan-F-TBRS: pan-tissue fibroblast TGF-β response genes; SCCL, basal/SCC-like; T_{eff}: CD8 T effector signature; TMB: tumour mutation burden; UroA, urothelial-like A; UroB, urothelial-like B.

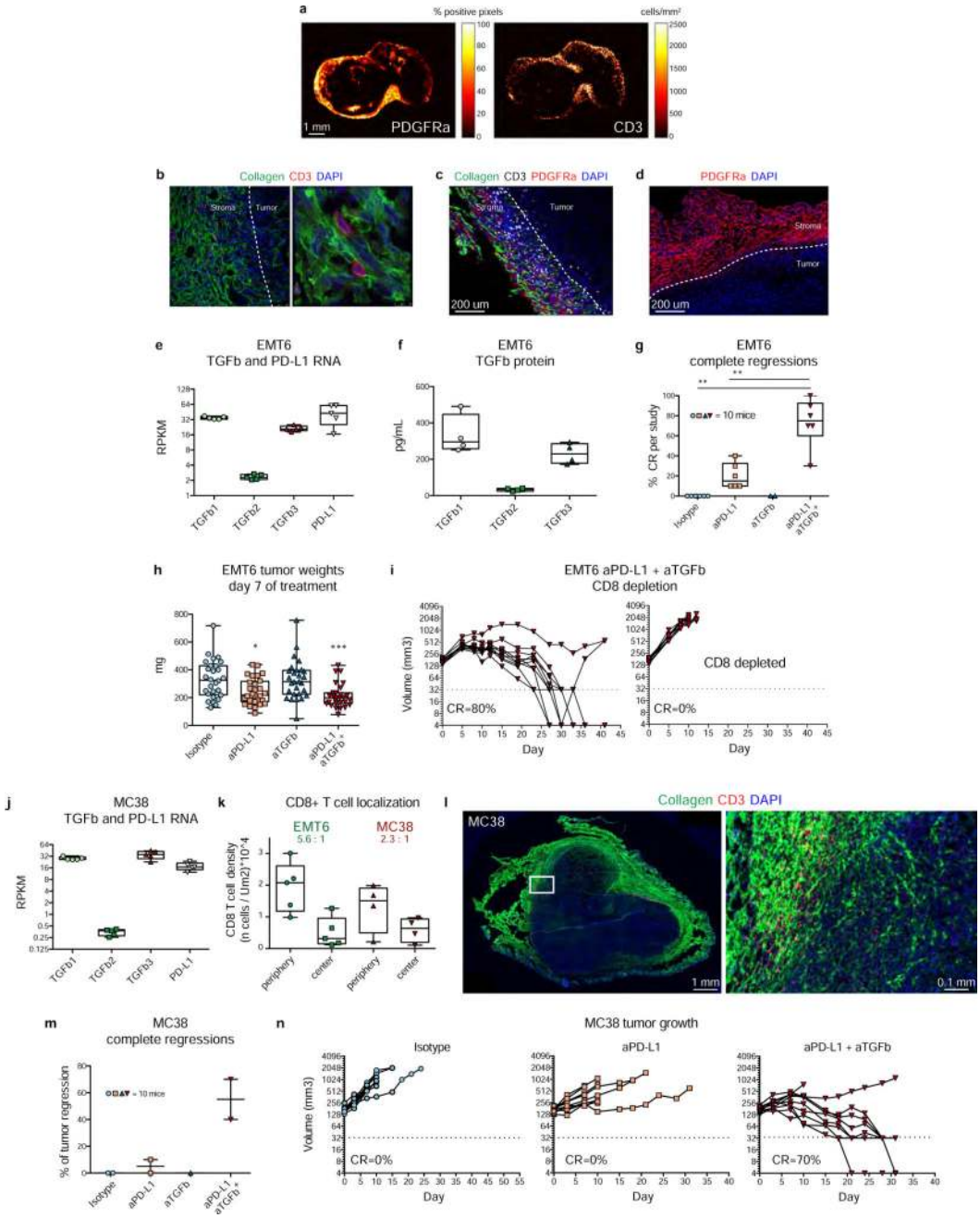

Extended Data Figure 5. Efficacy data of anti–TGF-β + anti–PD-L1 treatment in EMT6 and MC38 immune excluded tumour models

a, Fibroblast (PDGFRa, left panel) and T cell (CD3, right panel) parametric maps. Left image shows PDGFRa density (% positive pixels) and right shows T-cell density (cells/mm^2). Scale bar: 1 millimetre. Representative images of eight biological replicates. **b,**

Collagen (green) and T cells (CD3, red) stained by immunofluorescence. Representative images of five biological replicates. **c**, Collagen (green), T cells (CD3, white) and PDGFRa (red) in EMT6 tumours stained by immunofluorescence. Scale bar: 200 microns. **d,** PDGFRa (red) in EMT6 tumours stained by immunofluorescence. Scale bar: 200 microns. Representative images of four biological replicates. **e,** Quantification of TGF-β and PD-L1 RNA in whole EMT6 tumours by RNAseq. The tumours were inoculated orthotopically and collected when volume reached 300 mm^3 ($n = 5$ mice; data from one experiment). **f,** Quantification of TGF-β protein within whole EMT6 tumours by ELISA. Tumours were collected 14 days after inoculation, flash frozen and lysed for protein quantification ($n = 4$ mice; data from one experiment). **g,** Balbc mice were inoculated with EMT6 tumour cells orthotopically. When tumour volumes reached ≈ 160 mm^3 approximately nine days after inoculation, mice were treated with isotype control, anti–PD-L1, anti–TGF-β, or a combination of anti–PD-L1 with anti–TGF-β. Tumours were measured two times per week for approximately eight weeks by calliper. When tumour volumes fell below 32 mm^3 (lowest limit of detection), they were considered complete response. Percentage of complete regressions across 2–6 independent studies (10 mice/group per study). **h**, Tumour weights at day 7 after initiation of treatment ($n = 28$ mice per treatment group; data from three independent experiments). **i,** CD8 depletion experiment. CD8 T cells were depleted before initiation of treatment. **j,** Quantification of TGF-β and PD-L1 RNA in whole MC38 tumours by RNAseq. The tumours were inoculated subcutaneously and collected when volume reached 300 mm^3 ($n = 5$ mice; data from one experiment). **k,** Quantification of CD8 T cells in the centre and in the periphery of EMT6 and MC38 tumours from IHC stains. Data expressed as number of cells per tissue area (periphery is defined as 400–600 micron from the tumour edge, centre is the remaining distance to centre point). EMT6: $n = 5$ mice, MC38: $n = 4$ mice. **l,** Collagen (green) and T cells (CD3, red) in MC38 tumours stained by immunofluorescence. Scale bar, 1mm (left); 0.1mm (right). **m,** C57BL6 mice were inoculated with MC38 tumour cells subcutaneously. When tumour volumes reached ≈ 180 mm^3 approximately eight days after inoculation, mice were treated with isotype control, anti–PD-L1, anti–TGF-β, or a combination of anti–PD-L1 with anti–TGF-β. Tumours were measured two times per week for approximately eight weeks by calliper. When tumour volumes fell below 32 mm^3 (lowest limit of detection), they were considered complete response. Percentage of CR across 2 independent studies (1 for anti–TGF-β alone) shown with 10 mice per treatment group for each independent study. **n,** Tumour growth curves for each individual mouse are shown. The data are from one representative of two independent experiments with 10 mice per treatment group. All statistics are two-sided Mann-Whitney test compared to isotype group. * $p < 0.05$; ** $p < 0.01$; *** $p < 0.001$; **** $p < 0.0001$.

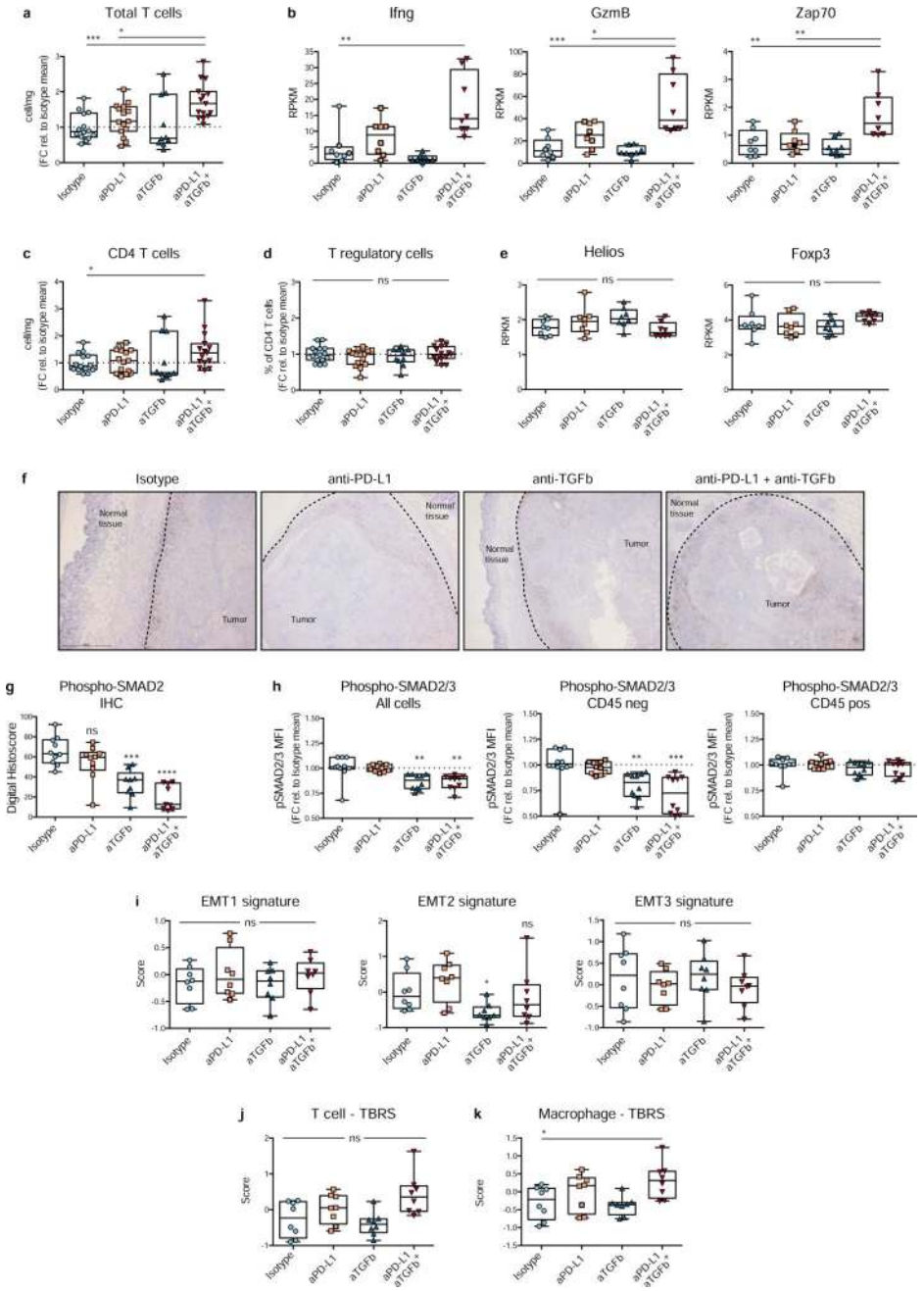

Extended Data Figure 6. Changes in TME following anti–TGF-β + anti–PD-L1 treatment in EMT6 tumours

a, c, d, Cytofluorimetric analysis of T cells seven days after initiation of the treatment. The abundance of total T cells (a), total CD4+ cells (c) and the percentage of T regulatory cells (CD25+FOXP3+) in the CD4+ population (d) are shown. $n = 15$ mice for all treatment groups except for anti-TGF-β alone in which $n = 10$, data combined from three independent experiments expressed as fold change relative to the isotype cell/mg average. **b**, **e**, RNAseq analysis on whole tumours collected seven days after the initiation of treatment. Single-gene expression for IFNg, GzmB and Zap70 (b) Helios and Foxp3 (e) are shown ($n = 8$ mice per treatment group; data from one experiment). **f,** Distribution of tumour-infiltrating

lymphocytes in tumours (T) as assessed by immunohistochemistry and digital imaging seven days after the initiation of treatment as above. Representative CD3 staining (brown). Dashed line indicates tumour boundaries. (n = 19 for all groups except anti–PD-L1/anti–TGF-β, in which n = 20; three independent experiments). Scale bar, 500 micron. **g,** Phospho-SMAD2 quantification by IHC at day 7 after initiation of treatment. (n = 9 or 10 mice per treatment groups; data from one experiment). **h,** Phosphoflow analysis of SMAD2/3 in tumours seven days after the initiation of treatment as above. Mean fluorescence intensity (MFI) of phospho-SMAD2/3 among total cells, CD45- or CD45+ cells are shown. Data are expressed as fold change (FC) relative to the isotype MFI average. 10 mice per treatment group from two independent experiments. **i–k**, RNAseq analysis on whole tumours collected seven days after the initiation of treatment. Three EMT signatures (i) as well as TGF-β response signatures for T cells (j) and macrophages (k) are also shown. (n = 8 mice per treatment group; data from one experiment). All statistics in the figure are two-sided Mann-Whitney test. * $p < 0.05$; ** $p < 0.01$; *** $p < 0.001$; ns, not significant compared to Isotype group.

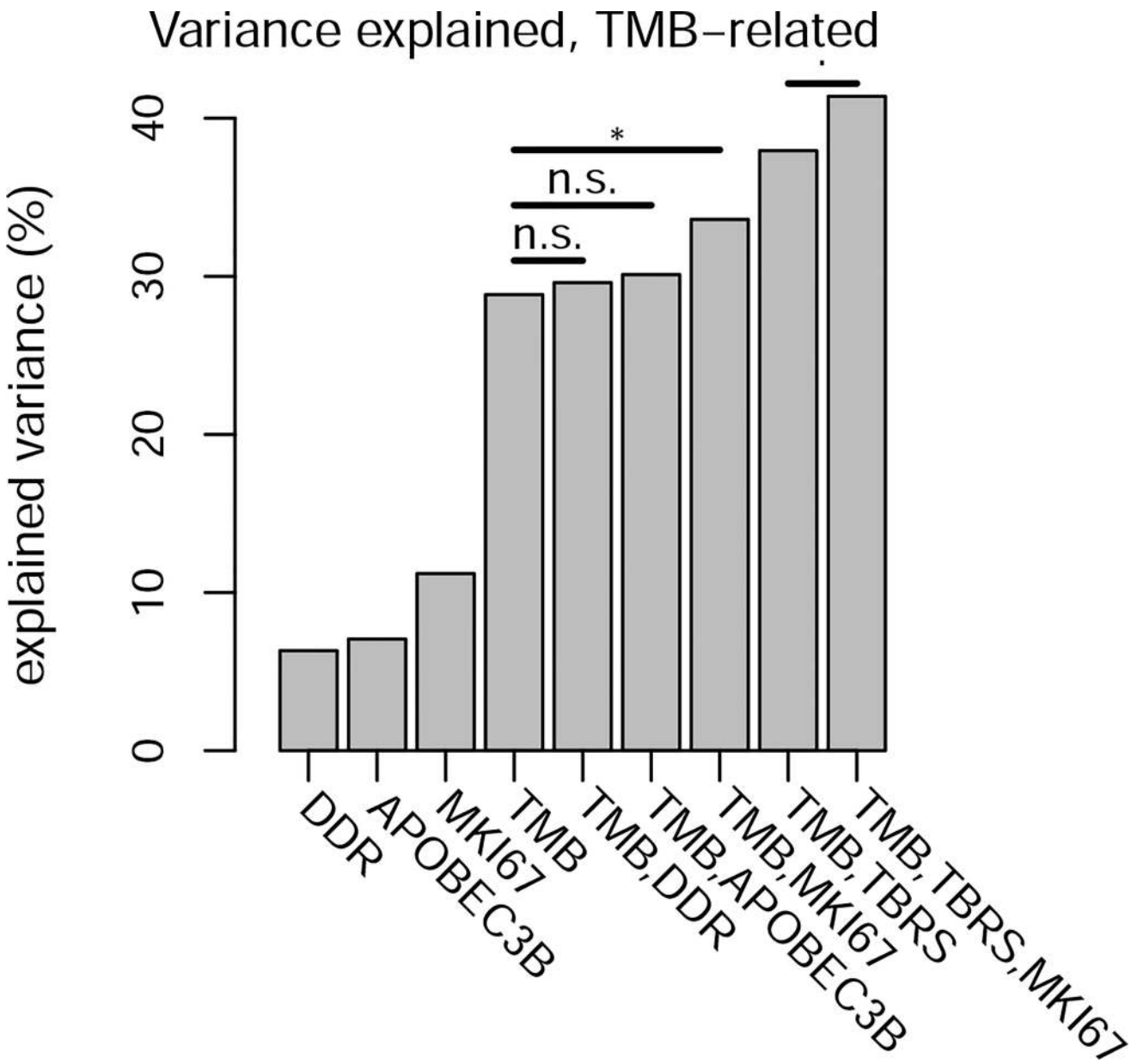

Extended Data Figure 7. Explained variance in patient response

Generalized linear models were fit using binary response (complete or partial response vs. stable or progressive disease) as the dependent variable and scores from single input or input combinations (x-axis) as independent variables (number of samples: 236). Percent explained variance of response is plotted on the y-axis. Comparisons between different models were made via likelihood ratio test; a significant *p* value means that the additional variable contributed some independent information to the model. TMB's association with response is significantly stronger than that of its proxy measurements (*APOBEC3B* and *MKI67* expression or mutation in members of the DDR set). *APOBEC3B* and DDR gene set mutation provided no additional explanatory information independent of direct measurement of TMB. Combining TMB with MKI67 expression did marginally improve on TMB alone, possibly through *MKI67*'s negative association with TFG-β (Extended Data Fig. 1e,f). To

test this hypothesis, we added *MKI67* to a two-pathway model based on TMB and the Pan-F-TBRS, and confirmed that *MKI67* does not add independent information to this two-pathway model. Further, there was no benefit from adding *MKI67* to our full three-pathway model, shown in Fig. 2f and Extended Data Fig. 2g. DDR: DNA damage repair; TBRS: pan-tissue fibroblast TGF-β response genes; TMB, tumour mutation burden. n.s. $p > 0.1$; · $p < 0.1$; * $p < 0.05$. Exact likelihood ratio test p values: "TMB,DDR" versus "TMB": 0.38, "TMB,APOBEC3B" versus "TMB": 0.26, "TMB,MKI67" versus "TMB": 0.029, "TMB,TBRS,MKI67" versus "TMB,TBRS": 0.064.

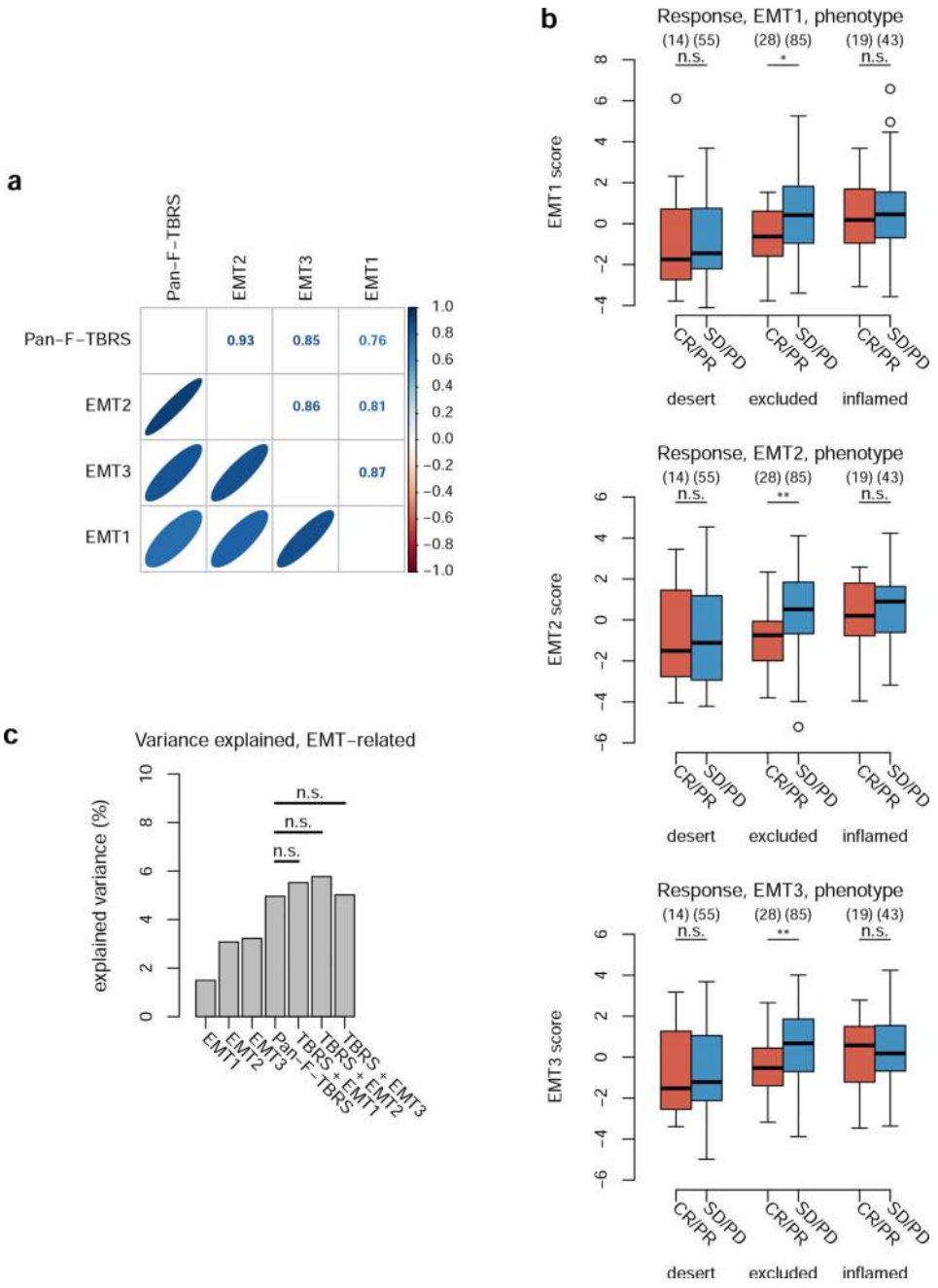

Extended Data Figure 8. Relationship between different TGF-β related gene expression signatures and response

a, Correlation between different TGF-β related gene expression signatures. In the left corner, correlation between signature scores/gene expression is visualized, calculated based on the complete RNA sequencing data set of 348 samples. In the right corner, Pearson correlation coefficients are given. Gene set membership is given in Supplementary Table S8. See Methods for computation of signature scores. **b,** EMT signature expression is associated with response to atezolizumab in excluded tumours. Scores of three different EMT signatures—EMT1[31], EMT2[32] and EMT3[33]—are significantly higher in non-responders (stable and progressive disease; SD/PD) than responders (complete and partial response; CR/PR) in excluded tumours (EMT1: $p = 0.0102$; EMT2: $p = 0.0027$: EMT3: $p = 0.0063$): there is no significant difference in signature scores in desert and inflamed tumours (all $p = 1$; two-tailed t test p values for each signature are Bonferroni corrected for 3 tests). The numbers above the graphs specify sample numbers in each bin. **c,** Explained variance in patient response. Generalized linear models were fit using binary response (complete or partial response vs. stable or progressive disease) as the dependent variable and scores from single input or input combinations (x-axis) as independent variables (number of samples: 233). Percent explained variance of response is plotted on the y-axis. Comparisons between different models were made via likelihood ratio test; a significant p value means that the additional variable contributed some independent information to the model. The Pan-F-TBRS's association with response is the strongest among its correlates, i.e., three different epithelial-to-mesenchymal transition (EMT) signatures. None of these signatures provided additional explanatory information independent of Pan-F-TBRS. (Pan-F-)TBRS: pan tissue fibroblast TGF-β response signature, EMT: epithelial-to-mesenchymal transition.

Supplementary Material

Refer to Web version on PubMed Central for supplementary material.

Acknowledgments

The authors would like to thank the patients and their families. We also thank all of the investigators and their staff involved in IMvigor210 study. We also thank C. Ahearn, Shari Lau, Charles Havnar, Zachary Boyd, Shruthi Sampath, Deanna Wilson, Jennifer Doss and medical writers at Health Interactions.

Dan Halligan & Loan Somarriba: Employees of Fios Genomics Ltd, a contract research organisation contracted to provide bioinformatics services to Genentech Inc. Michiel van der Heijden, Yohann Loriot and Thomas Powles have advisory roles for Roche/Genentech. Jonathan Rosenberg is a consultant for Roche/Genentech, BMS, Merck, AstraZeneca, EMD-Serono and research funding to his institution has been provided by Roche/Genentech. All other authors are employees and stockholders of Genentech/Roche.

Funding

Dr. Rosenberg acknowledges support from P30 CA008748.

References

1. Herbst RS, Soria J-C, Kowanetz M, Fine GD, Hamid O, Gordon MS, Sosman JA, McDermott DF, Powderly JD, Gettinger SN, Kohrt HEK, Horn L, Lawrence DP, Rost S, Leabman M, Xiao Y, Mokatrin A, Koeppen H, Hegde PS, Mellman I, Chen DS, Hodi FS. Predictive correlates of response to the anti-PD-L1 antibody MPDL3280A in cancer patients. Nature. 2014; 515:563–567. [PubMed: 25428504]

2. Powles T, Eder JP, Fine GD, Braiteh FS, Loriot Y, Cruz C, Bellmunt J, Burris HA, Petrylak DP, Teng S-L, Shen X, Boyd Z, Hegde PS, Chen DS, Vogelzang NJ. MPDL3280A (anti-PD-L1) treatment leads to clinical activity in metastatic bladder cancer. Nature. 2014; 515:558–562. [PubMed: 25428503]

3. Bellmunt J, de Wit R, Vaughn DJ, Fradet Y, Lee J-L, Fong L, Vogelzang NJ, Climent MA, Petrylak DP, Choueiri TK, Necchi A, Gerritsen W, Gurney H, Quinn DI, Culine S, Sternberg CN, Mai Y, Poehlein CH, Perini RF, Bajorin DF. KEYNOTE-045 Investigators. Pembrolizumab as Second-Line Therapy for Advanced Urothelial Carcinoma. N Engl J Med. 2017; 376:1015–1026. [PubMed: 28212060]

4. Rosenberg JE, Hoffman-Censits J, Powles T, van der Heijden MS, Balar AV, Necchi A, Dawson N, O'Donnell PH, Balmanoukian A, Loriot Y, Srinivas S, Retz MM, Grivas P, Joseph RW, Galsky MD, Fleming MT, Petrylak DP, Perez-Gracia JL, Burris HA, Castellano D, Canil C, Bellmunt J, Bajorin D, Nickles D, Bourgon R, Frampton GM, Cui N, Mariathasan S, Abidoye O, Fine GD, Dreicer R. Atezolizumab in patients with locally advanced and metastatic urothelial carcinoma who have progressed following treatment with platinum-based chemotherapy: a single-arm, multicentre, phase 2 trial. Lancet. 2016; 387:1909–1920. [PubMed: 26952546]

5. Balar AV, Galsky MD, Rosenberg JE, Powles T, Petrylak DP, Bellmunt J, Loriot Y, Necchi A, Hoffman-Censits J, Perez-Gracia JL, Dawson NA, van der Heijden MS, Dreicer R, Srinivas S, Retz MM, Joseph RW, Drakaki A, Vaishampayan UN, Sridhar SS, Quinn DI, Durán I, Shaffer DR, Eigl BJ, Grivas PD, Yu EY, Li S, Kadel EE, Boyd Z, Bourgon R, Hegde PS, Mariathasan S, Thåström A, Abidoye OO, Fine GD, Bajorin DF. IMvigor210 Study Group. Atezolizumab as first-line treatment in cisplatin-ineligible patients with locally advanced and metastatic urothelial carcinoma: a single-arm, multicentre, phase 2 trial. Lancet. 2017; 389:67–76. [PubMed: 27939400]

6. Alexandrov LB, Nik-Zainal S, Wedge DC, Aparicio SAJR, Behjati S, Biankin AV, Bignell GR, Bolli N, Borg A, Børresen-Dale A-L, Boyault S, Burkhardt B, Butler AP, Caldas C, Davies HR, Desmedt C, Eils R, Eyfjörd JE, Foekens JA, Greaves M, Hosoda F, Hutter B, Ilicic T, Imbeaud S, Imielinski M, Imielinsk M, Jäger N, Jones DTW, Jones D, Knappskog S, Kool M, Lakhani SR, López-Otín C, Martin S, Munshi NC, Nakamura H, Northcott PA, Pajic M, Papaemmanuil E, Paradiso A, Pearson JV, Puente XS, Raine K, Ramakrishna M, Richardson AL, Richter J, Rosenstiel P, Schlesner M, Schumacher TN, Span PN, Teague JW, Totoki Y, Tutt ANJ, Valdés-Mas R, van Buuren MM, van 't Veer LJ, Vincent-Salomon A, Waddell N, Yates LR, Australian Pancreatic Cancer Genome Initiative, ICGC Breast Cancer Consortium, ICGC MMML-Seq Consortium, ICGC PedBrain. Zucman-Rossi J, Futreal PA, McDermott U, Lichter P, Meyerson M, Grimmond SM, Siebert R, Campo E, Shibata T, Pfister SM, Campbell PJ, Stratton MR. Signatures of mutational processes in human cancer. Nature. 2013; 500:415–421. [PubMed: 23945592]

7. Chalmers ZR, Connelly CF, Fabrizio D, Gay L, Ali SM, Ennis R, Schrock A, Campbell B, Shlien A, Chmielecki J, Huang F, He Y, Sun J, Tabori U, Kennedy M, Lieber DS, Roels S, White J, Otto GA, Ross JS, Garraway L, Miller VA, Stephens PJ, Frampton GM. Analysis of 100,000 human cancer genomes reveals the landscape of tumor mutational burden. Genome Med. 2017; 9:34. [PubMed: 28420421]

8. Snyder A, Makarov V, Merghoub T, Yuan J, Zaretsky JM, Desrichard A, Walsh LA, Postow MA, Wong P, Ho TS, Hollmann TJ, Bruggeman C, Kannan K, Li Y, Elipenahli C, Liu C, Harbison CT, Wang L, Ribas A, Wolchok JD, Chan TA. Genetic basis for clinical response to CTLA-4 blockade in melanoma. N Engl J Med. 2014; 371:2189–2199. [PubMed: 25409260]

9. Rizvi NA, Hellmann MD, Snyder A, Kvistborg P, Makarov V, Havel JJ, Lee W, Yuan J, Wong P, Ho TS, Miller ML, Rekhtman N, Moreira AL, Ibrahim F, Bruggeman C, Gasmi B, Zappasodi R, Maeda Y, Sander C, Garon EB, Merghoub T, Wolchok JD, Schumacher TN, Chan TA. Cancer immunology. Mutational landscape determines sensitivity to PD-1 blockade in non-small cell lung cancer. Science. 2015; 348:124–128. [PubMed: 25765070]

10. Van Allen EM, Miao D, Schilling B, Shukla SA, Blank C. Genomic correlates of response to CTLA-4 blockade in metastatic melanoma. Science. 2015; 350:203–207. [PubMed: 26450211]

11. Chen DS, Mellman I. Oncology meets immunology: the cancer-immunity cycle. Immunity. 2013; 39:1–10. [PubMed: 23890059]

12. The Cancer Genome Atlas Research. Comprehensive molecular characterization of urothelial bladder carcinoma. Nature. 2014; 507:315–322. [PubMed: 24476821]

13. Burns MB, Temiz NA, Harris RS. Evidence for APOBEC3B mutagenesis in multiple human cancers. Nat Genet. 2013; 45:977–983. [PubMed: 23852168]

14. Gao J, Shi LZ, Zhao H, Chen J, Xiong L, He Q, Chen T, Roszik J, Bernatchez C, Woodman SE, Chen P-L, Hwu P, Allison JP, Futreal A, Wargo JA, Sharma P. Loss of IFN-γ Pathway Genes in Tumor Cells as a Mechanism of Resistance to Anti-CTLA-4 Therapy. Cell. 2016; 167:397–404.e9. [PubMed: 27667683]

15. Zaretsky JM, Garcia-Diaz A, Shin DS, Escuin-Ordinas H, Hugo W, Hu-Lieskovan S, Torrejon DY, Abril-Rodriguez G, Sandoval S, Barthly L, Saco J, Homet Moreno B, Mezzadra R, Chmielowski B, Ruchalski K, Shintaku IP, Sanchez PJ, Puig-Saus C, Cherry G, Seja E, Kong X, Pang J, Berent-Maoz B, Comin-Anduix B, Graeber TG, Tumeh PC, Schumacher TNM, Lo RS, Ribas A. Mutations Associated with Acquired Resistance to PD-1 Blockade in Melanoma. N Engl J Med. 2016; 375:819–829. [PubMed: 27433843]

16. Ribas A. Adaptive Immune Resistance: How Cancer Protects from Immune Attack. Cancer Discov. 2015; 5:915–919. [PubMed: 26272491]

17. Benci JL, Xu B, Qiu Y, Wu TJ, Dada H, Twyman-Saint Victor C, Cucolo L, Lee DSM, Pauken KE, Huang AC, Gangadhar TC, Amaravadi RK, Schuchter LM, Feldman MD, Ishwaran H, Vonderheide RH, Maity A, Wherry EJ, Minn AJ. Tumor Interferon Signaling Regulates a Multigenic Resistance Program to Immune Checkpoint Blockade. Cell. 2016; 167:1540–1554.e12. [PubMed: 27912061]

18. Lin R-L, Zhao L-J. Mechanistic basis and clinical relevance of the role of transforming growth factor-β in cancer. Cancer Biol Med. 2015; 12:385–393. [PubMed: 26779375]

19. Massagué J. TGFbeta in Cancer. Cell. 2008; 134:215–230. [PubMed: 18662538]

20. Calon A, Lonardo E, Berenguer-Llergo A, Espinet E, Hernando-Momblona X, Iglesias M, Sevillano M, Palomo-Ponce S, Tauriello DVF, Byrom D, Cortina C, Morral C, Barceló C, Tosi S, Riera A, Attolini CS-O, Rossell D, Sancho E, Batlle E. Stromal gene expression defines poor-prognosis subtypes in colorectal cancer. Nat Genet. 2015; 47:320–329. [PubMed: 25706628]

21. Derynck R, Zhang YE. Smad-dependent and Smad-independent pathways in TGF-beta family signalling. Nature. 2003; 425:577–584. [PubMed: 14534577]

22. Morikawa M, Derynck R, Miyazono K. TGF-β and the TGF-β Family: Context-Dependent Roles in Cell and Tissue Physiology. Cold Spring Harb Perspect Biol. 2016; 8:a021873. [PubMed: 27141051]

23. Flavell RA, Sanjabi S, Wrzesinski SH, Licona-Limón P. The polarization of immune cells in the tumour environment by TGFbeta. Nature Reviews Immunology. 2010; 10:554–567.

24. Hegde PS, Karanikas V, Evers S. The Where, the When, and the How of Immune Monitoring for Cancer Immunotherapies in the Era of Checkpoint Inhibition. Clin Cancer Res. 2016; 22:1865–1874. [PubMed: 27084740]

25. Tumeh PC, Harview CL, Yearley JH, Shintaku IP, Taylor EJM, Robert L, Chmielowski B, Spasic M, Henry G, Ciobanu V, West AN, Carmona M, Kivork C, Seja E, Cherry G, Gutierrez AJ, Grogan TR, Mateus C, Tomasic G, Glaspy JA, Emerson RO, Robins H, Pierce RH, Elashoff DA, Robert C, Ribas A. PD-1 blockade induces responses by inhibiting adaptive immune resistance. Nature. 2014; 515:568–571. [PubMed: 25428505]

26. Dobson, AJ., Barnett, AG. An Introduction to Generalized Linear Models, Third Edition. Chapman & Hall/CRC Press; 2008.

27. Sjödahl G, Lauss M, Lövgren K, Chebil G, Gudjonsson S, Veerla S, Patschan O, Aine M, Fernö M, Ringnér M, Månsson W, Liedberg F, Lindgren D, Höglund M. A molecular taxonomy for urothelial carcinoma. Clin Cancer Res. 2012; 18:3377–3386. [PubMed: 22553347]

28. Sjödahl G, Lövgren K, Lauss M, Patschan O, Gudjonsson S, Chebil G, Aine M, Eriksson P, Månsson W, Lindgren D, Fernö M, Liedberg F, Höglund M. Toward a molecular pathologic classification of urothelial carcinoma. Am. J. Pathol. 2013; 183:681–691. [PubMed: 23827819]

29. Rusinova I, Forster S, Yu S, Kannan A, Masse M, Cumming H, Chapman R, Hertzog PJ. Interferome v2.0: an updated database of annotated interferon-regulated genes. Nucleic Acids Res. 2013; 41:D1040–6. [PubMed: 23203888]

30. Spranger S, Bao R, Gajewski TF. Melanoma-intrinsic β-catenin signalling prevents anti-tumour immunity. Nature. 2015; 523:231–235. [PubMed: 25970248]

31. Damrauer JS, Hoadley KA, Chism DD, Fan C, Tiganelli CJ, Wobker SE, Yeh JJ, Milowsky MI, Iyer G, Parker JS, Kim WY. Intrinsic subtypes of high-grade bladder cancer reflect the hallmarks of breast cancer biology. Proc Natl Acad Sci U S A. 2014; 111:3110–3115. [PubMed: 24520177]

32. Hugo W, Zaretsky JM, Sun L, Song C, Moreno BH, Hu-Lieskovan S, Berent-Maoz B, Pang J, Chmielowski B, Cherry G, Seja E, Lomeli S, Kong X, Kelley MC, Sosman JA, Johnson DB, Ribas A, Lo RS. Genomic and Transcriptomic Features of Response to Anti-PD-1 Therapy in Metastatic Melanoma. Cell. 2016; 165:35–44. [PubMed: 26997480]

33. Hedegaard J, Lamy P, Nordentoft I, Algaba F, Høyer S, Ulhøi BP, Vang S, Reinert T, Hermann GG, Mogensen K, Thomsen MBH, Nielsen MM, Marquez M, Segersten U, Aine M, Höglund M, Birkenkamp-Demtröder K, Fristrup N, Borre M, Hartmann A, Stöhr R, Wach S, Keck B, Seitz AK, Nawroth R, Maurer T, Tulic C, Simic T, Junker K, Horstmann M, Harving N, Petersen AC, Calle ML, Steyerberg EW, Beukers W, van Kessel KEM, Jensen JB, Pedersen JS, Malmström P-U, Malats N, Real FX, Zwarthoff EC, Ørntoft TF, Dyrskjøt L. Comprehensive Transcriptional Analysis of Early-Stage Urothelial Carcinoma. Cancer Cell. 2016; 30:27–42. [PubMed: 27321955]

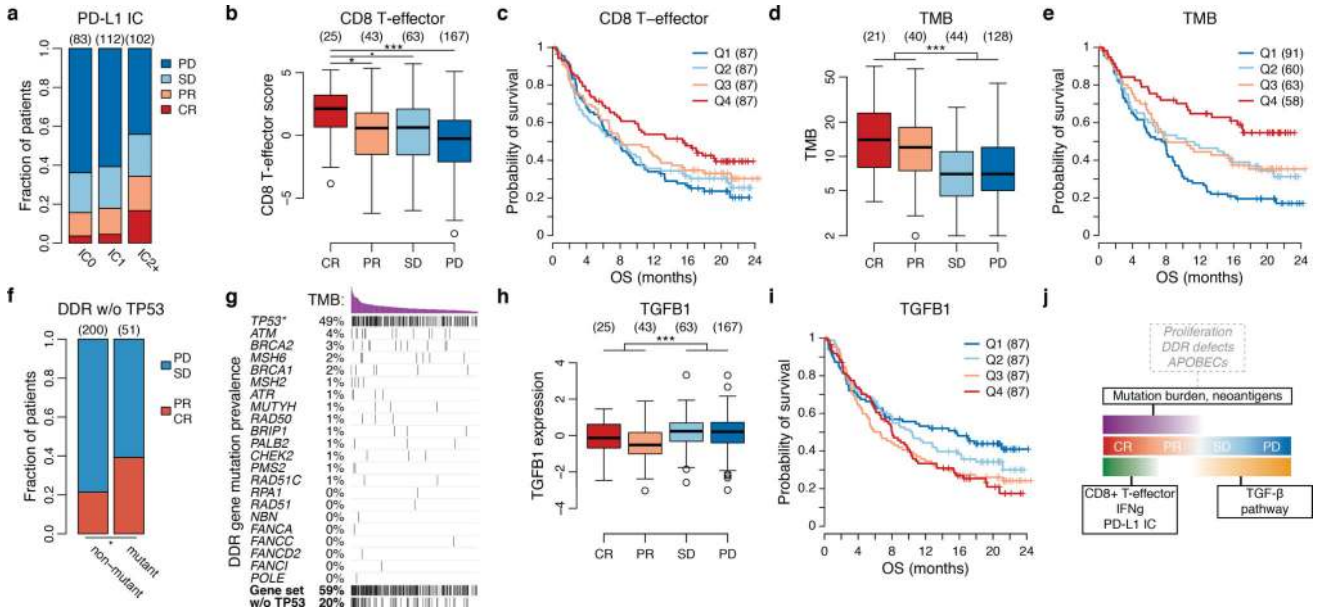

Figure 1. Three core biological pathways are associated with response to atezolizumab

a, PD-L1 IC was associated with response (two-sided Fisher exact test $p = 0.0038$). IC2+ tumours had a significantly higher CR rate ($p = 0.0006$). **b,** CD8+ T_{eff} signature score is positively associated with response (two-tailed t test $p = 0.0087$), with association driven by the CR group (CR vs PR $p = 0.0388$, CR vs SD $p = 0.0668$, CR vs PD $p = 0.0003$). **c,** CD8+ T_{eff} signature quartiles (Q1: lowe are significantly associated with overall survival (likelihood ratio test $p = 0.0092$). **d–e,** TMB is positively associated with response to atezolizumab (two-tailed t test $p = 6.9 \times 10^{-7}$) and overall survival (likelihood ratio test $p = 2.0 \times 10^{-5}$). A similar plot for tumour neoantigen burden is given in Extended Data Fig. 1e,f. **f–g,** There is a significant association between DDR mutation status and (f) response (two-sided Fisher exact test $p = 0.0117$ excluding *TP53*) and (g) TMB, both with (two-sided Fisher exact test $p = 6.01 \times 10^{-8}$) and without inclusion of *TP53* ($p = 1.95 \times 10^{-5}$) **h–i,** *TGFB1* gene expression is significantly associated with non-response (two-tailed t test $p = 0.00011$) and reduced overall survival (likelihood ratio test $p = 0.0096$). **j,** The relationship between response and three core biological pathways. · $p < 0.10$; * $p < 0.05$; ** $p < 0.01$; *** $p < 0.001$. Sample sizes given in parentheses. Q1: lowest quartile, Q4: highest quartile.

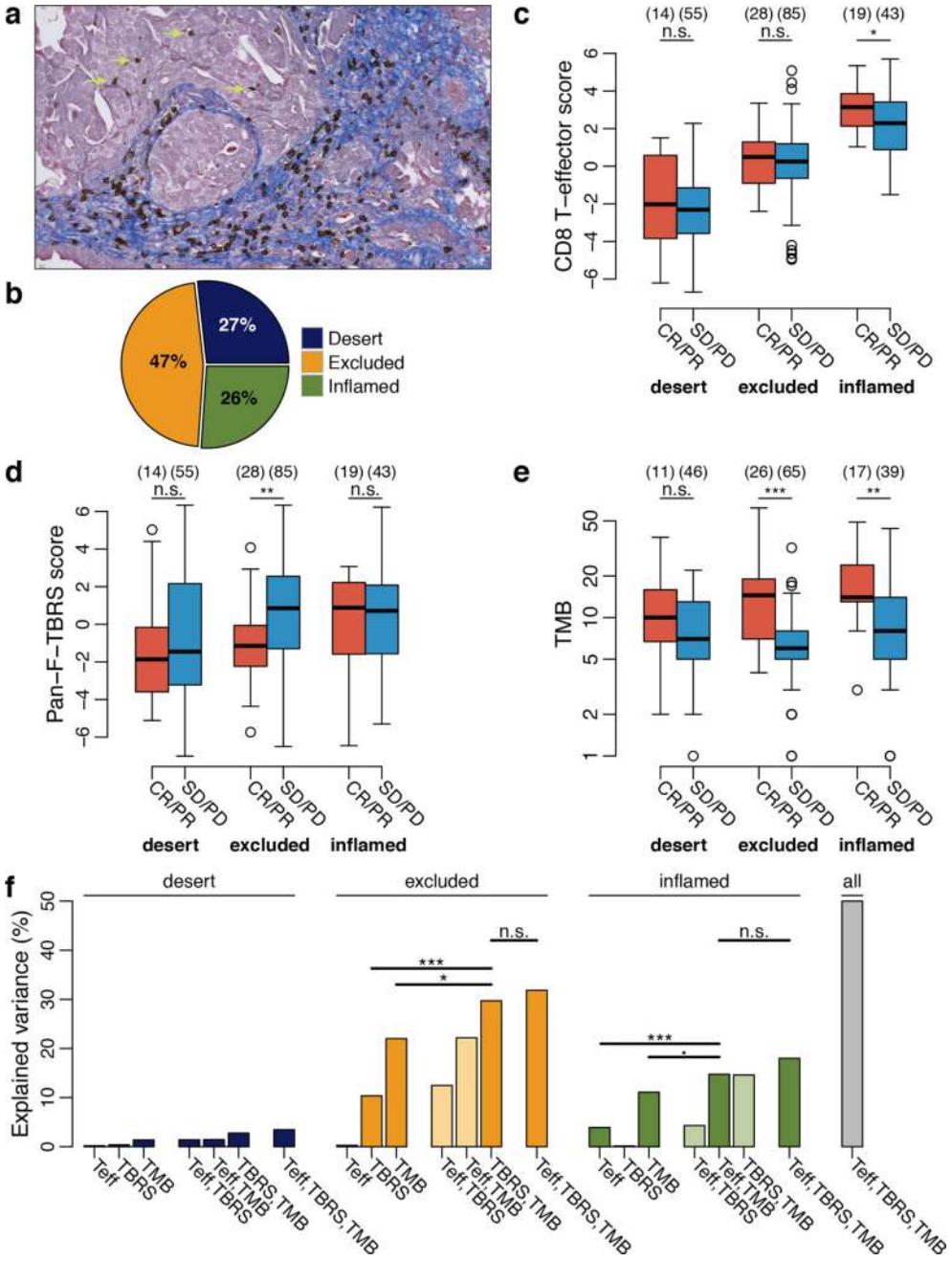

Figure 2. TGF-β is associated with lack of response in the excluded tumour-immune phenotype

a, Combined CD8 IHC–trichrome stain. CD8+ T cells (DAB, brown) are primarily within collagenous stroma (blue). Rare CD8+ T cells are interspersed between tumour cells (green arrows). **b,** Distribution of tumour-immune phenotypes in IMvigor210. **c,** CD8+ T_{eff} score is significantly associated with response only in the inflamed phenotype (two-tailed t test $p =$ 0.042). **d,** Pan-F-TBRS is significantly associated with response only in the excluded phenotype (two-tailed t test $p = 0.0066$). **e,** TMB is significantly associated with response in the excluded and inflamed phenotypes (two-tailed t test $p = 0.00009$ and 0.00258). **f,** Explained variance in patient response for generalized linear models fit using single core

pathways or pathway combinations. In immune desert tumours ($n = 57$), core pathways showed negligible explanatory power. For excluded tumours ($n = 91$), Pan-F-TBRS and TMB were associated with response as singletons; combining the two provided statistically significant improvement over single terms (likelihood ratio $p = 6.23 \times 10^{-5}$ and 0.02125, respectively). For inflamed tumours ($n = 56$), CD8+ T_{eff} and TMB were associated with response as singletons; combining the two provided statistically significant improvement over single terms (likelihood ratio $p = 0.00099$ and 0.0557, respectively). Standard forward selection applied to all patients (grey) identified a three-pathway model as significantly better than all single- or two-pathway models (Extended Data Fig. 2g). n.s., nonsignificant; * $p < 0.05$; ** $p < 0.01$; *** $p < 0.001$. Sample sizes given in parentheses.

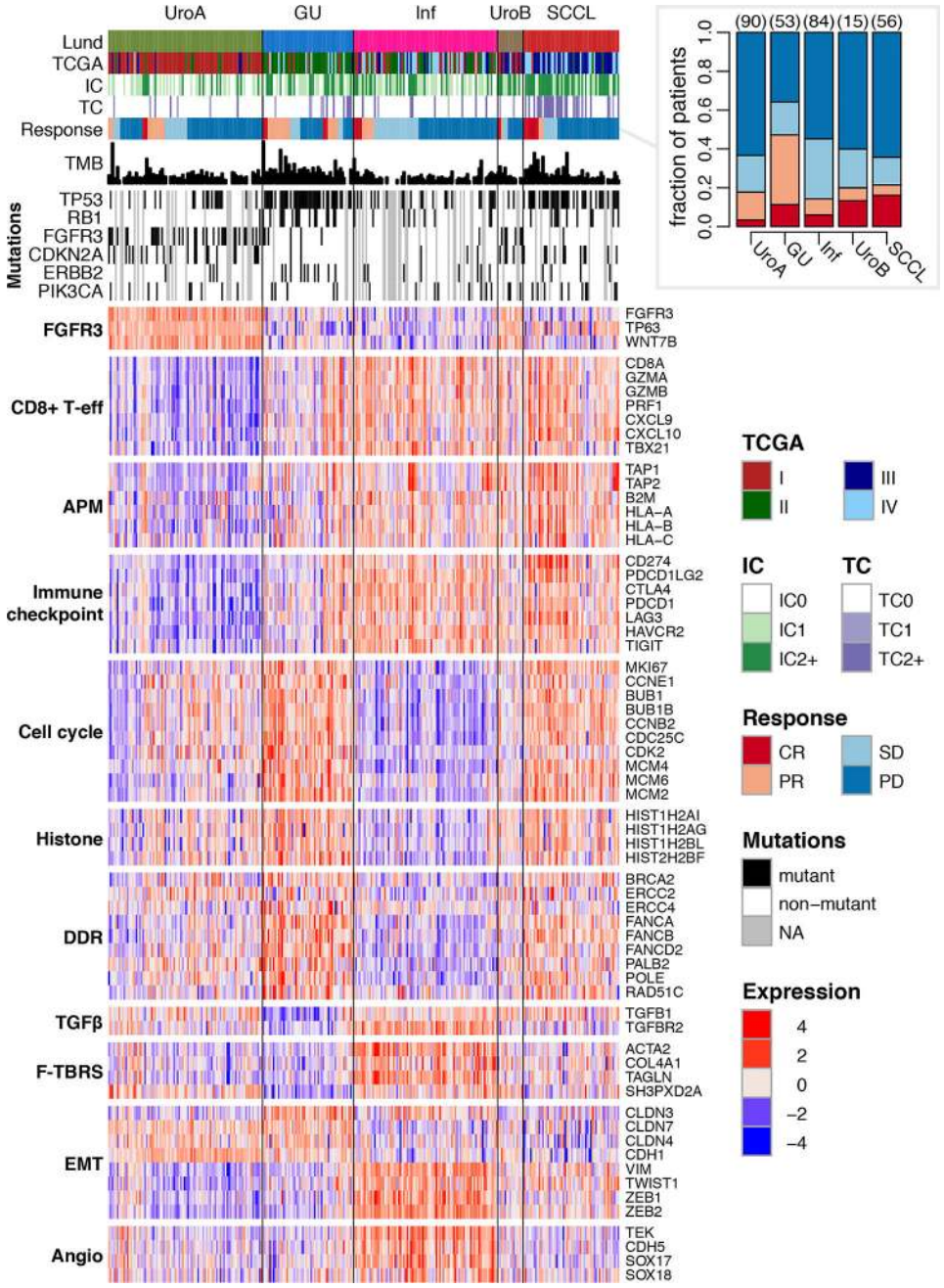

Figure 3. Relationship between molecular subtypes (Lund scheme) and core biological pathways

Rows of the heat map show gene expression (z-scores) grouped by pathway. Inset: response vs. Lund molecular subtype, showing that the genomically unstable (GU) subtype has a significantly higher response rate (two-sided Fisher exact test $p = 1.6 \times 10^{-5}$). Sample sizes given in parentheses.

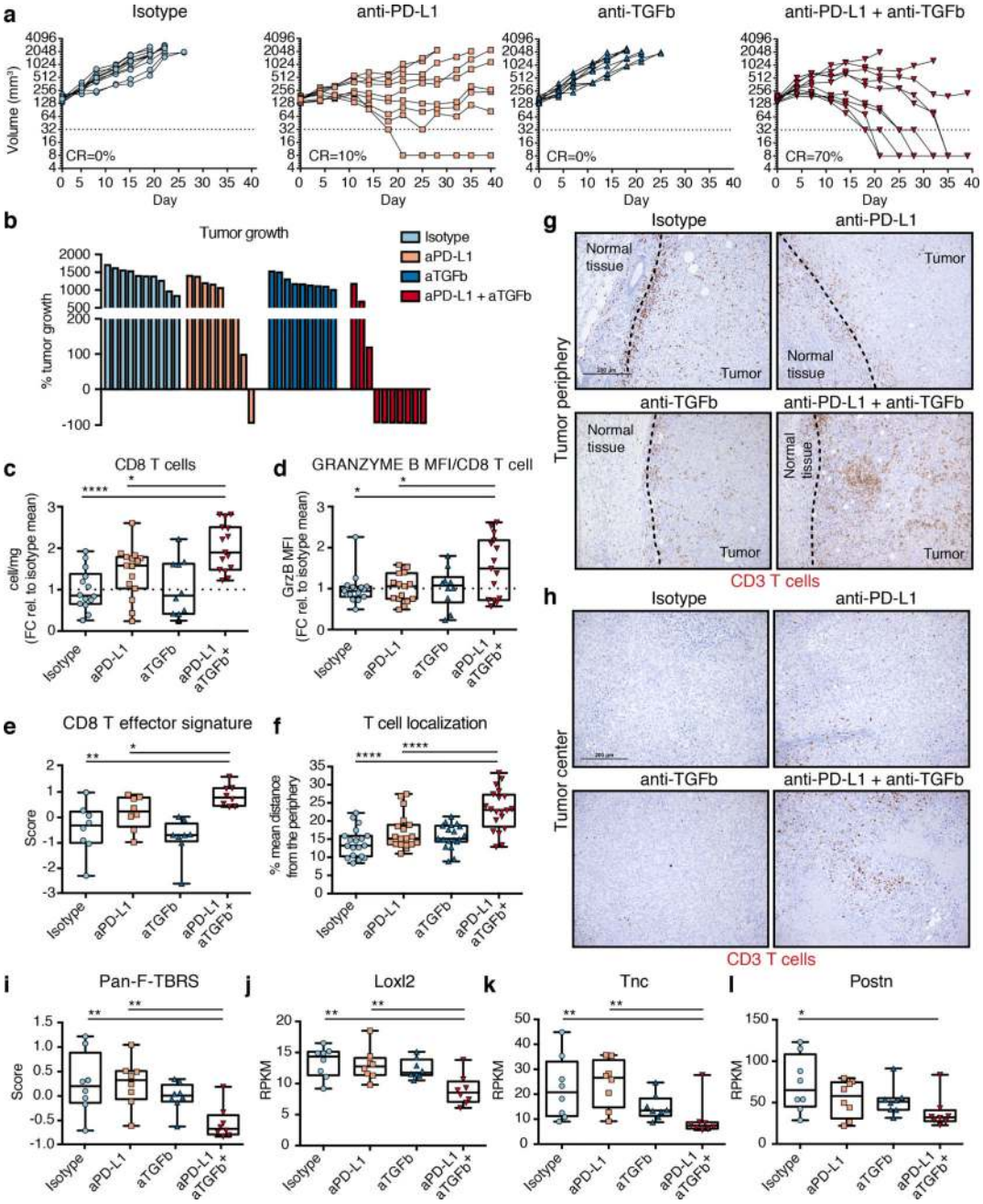

Figure 4. Tumour regression and changes in TME following therapeutic anti–TGF-β + anti–PD-L1 treatment in EMT6 tumours

a, Tumour growth curves. **b,** Change in tumour volume compared to baseline. (6 independent experiments, 10 mice per group.) **c–d,** Fold change (FC) in total CD8+ T cell abundance (c) and CD8+ T cell GRANZYME B MFI by flow cytometry (d). (3 independent experiments, $n = 15$ for all groups except anti–TGF-β, where $n = 10$.) **e,** CD8+ T_{eff} signature (1 experiment, $n = 8$ per group). **f,** TIL localisation quantification by immunohistochemistry (3 independent experiments, $n = 19$ for all groups except anti–PD-L1/anti–TGF-β, where $n = 20$; Tukey HSD multiple comparison adjustment). **g–h,** Representative CD3 staining of

tumour periphery (g) and centre (h). Scale bar is 200 microns. **i–l,** Pan-F-TBRS signature (i) and expression of fibroblast genes (j–l). (1 experiment, $n = 8$ per group.) All data shown in c–l from tumours collected at day 7 after treatment initiation. All p values based on two-sided Mann-Whitney tests unless otherwise indicated. * $p < 0.05$; ** $p < 0.01$; *** $p < 0.001$; **** $p < 0.0001$.